Iranian Journal of Science & Technology, Transaction B, Engineering, Vol. 34, No. B1, pp 63-80
Printed in The Islamic Republic of Iran, 2010

ZERO EXTENSION LINE METHOD FOR THREE-DIMENSIONAL STABILITY ANALYSIS IN SOIL ENGINEERING*

M. JAHANANDISH[1**] S. M. MANSOORZADEH[2] AND K. EMAD[2]

[1]Dept. of Civil Engineering, School of Engineering, Shiraz University, Shiraz, I. R. of Iran
Email: jahanand@shirazu.ac.ir
[2]Transportation Research Institute, Tehran, I. R. of Iran

Abstract– This paper presents a new approach for three-dimensional stability analysis of soils using the Zero Extension Line Method. The method assumes the intermediate principal stress-planes to be straight. The geometric considerations for obtaining the orientation of these planes in the plastic zone are described. The equilibrium-yield equations are integrated in these planes to give the total applicable load at the limiting equilibrium state. The method accounts for the nonasssociativity of soil behavior as well. It also considers the effect of partial mobilization of soil strength on the counter side of the slope, on its stability. Based on this method, a computer code, Slope3D8, has been written for three-dimensional stability analysis. Examples have been provided to show the capability of the model in analyzing three-dimensional stability of slopes under drained and undrained conditions. In-plan-curvature of slopes and the centrifugal force resulting from movement of vehicles in curved routes can also be modeled. The model predicts lower ultimate load as compared to the existing three dimensional limit analysis methods. Some of the difference in the results of these two models is due to the aggravating effect of counter side that is not considered by the developed three-dimensional limit analysis models. It has been concluded that the presented model provides a useful tool for three-dimensional stability analysis in soil engineering.

Keywords– Three-dimensional analysis, stability, characteristics, zero extension lines, curved slopes

1. INTRODUCTION

Most soil stability problems encountered in practice are three-dimensional rather than two-dimensional. The loading and geometric conditions of the problem and the material condition should remain the same along the third dimension in order to treat a problem two-dimensionally. These conditions rarely happen in practice. Nevertheless, two-dimensional analyses are used in most soil stability assessments because of their simplicity and the belief that they are always conservative. However, the three-dimensional nature of most practical problems together with the necessity of observing economic considerations in design have drawn attention to the three-dimensional methods of stability analysis. These methods are more or less the extensions of two-dimensional limit equilibrium and limit analysis methods to the three-dimensional case. As in the two dimensional case, most of the developed three dimensional models are based on limit equilibrium method (LEM). This is due to the versatility of this method in handling diverse soil and water conditions and the geometry of the problem. An early approach was to consider the 3D problem as an assembly of 2D ones. The 3D-safety factor is then obtained from the weighted average of their safety factors [1, 2]. Anagnosti's method can be considered the extension of Morgenstern-Price method to 3D [3]. Azzouz and Baligh extended Swedish circle method for 3D stability analysis of homogeneous slopes

*Received by the editors January 28, 2009; Accepted October 18, 2009.
**Corresponding author

[4, 5]. Gens et al. extended the circular arc (ϕ= 0) method to 3D for the homogeneous, isotropic, and purely cohesive slopes [6]. Hovland developed the ordinary method of columns which is the extension of the ordinary method of slices of Fellenius [7]. Chen and Chameau extended the Spencer's method to 3D [8]. A more advanced model based on that of Spencer's has also been developed by Chen et al. [9]. Jiang and Yamagami combined the same method with dynamic programming in search of the critical 3D slip surface [10]. Lechinsky et. al., have extended the variational based limit equilibrium approach to 3D [11, 12]. Extension of Janbu's method to 3D was made by Ugai and later by Byrene et al. [13, 14]. Hungr et. al.'s 3D model is based on Bishop simplified method [15]. Huang, and Tsai, and Huang et. al., made a further extension by considering the moment-equilibrium in transverse direction to handle asymmetric problems as well [16, 17]. It should be mentioned that in general, the formulation of the problem in LEM involves many degrees of indeterminacy and requires simplifying assumptions. This becomes more critical in 3D-problems because, more simplifying assumptions are required in this case to render the problem determinate; and this makes the results less reliable [10,18,19].

Limit analysis methods (LAM) have also been applied to slope stability analyses [19-22]. These methods are not as versatile as the limit equilibrium, but their results are more reliable because they use bound theorems of plasticity for associated materials. Approaches in 3D-modeling by limit analysis are limited to the upper bound method because of being simpler. An early approach to the problem was made by Giger and Kirizek who investigated the stability of vertical corner cuts [23]. Michlowski assessed the 3D stability of locally loaded slopes by the same approach [19]. Askari [20], and Farzaneh and Askari [21], improved Michalowski's assumed mechanism and applied a better optimization procedure for solution of the problem. They extended the LAM to a more general case of nonhomogeneous slopes [21]. Chen et. al. have also used the upper bound method of limit analysis for 3D slope stability analysis [24,25]. It has to be mentioned that, generally, soils are not an associated-flow rule material and the limit load is significantly lower for such a material. An attempt has been made to define an equivalent material with reduced values of c and ϕ, and to still use the limit theorems [26].

A true limiting equilibrium analysis of the stability of soil slopes has been made possible using the stress characteristics method (SCM) [27]. The method combines the differential equations of equilibrium with yield condition and uses the celebrated method of characteristics to solve the resulting quasi-linear partial differential equations. The method is not as versatile as the conventional limit equilibrium method because it uses a continuum approach for solution of the problem. Nevertheless, it has been a favorite one because it provides us with the ultimate load at which the equilibrium condition is still satisfied. Furthermore, because of being rigorous, it has been used as a benchmark for the evaluation of results of other methods in cases where solutions have been possible [28, 22, 29]. No consideration is made in this method to the nonassociative behavior of soil. Therefore, the obtained results are still not on the safe side unless we use equivalently reduced c and ϕ values in the analysis to account for nonassociativity. In the analysis of the stability of slopes; the method has only been used for the analysis of plane strain [30] and axisymmetric problems [31].

A more advanced method of stability analysis is the zero extension line method (ZELM) [32-36]. Although it uses the method of characteristics for solving the governing equations, it is based on the velocity characteristics (i.e., the zero extension lines) rather than the stress characteristics. The method considers the nonassociative behavior of soil at the limiting equilibrium state as well. Therefore, it is considered more general than the conventional method of stress characteristics. The zero extension line method has been developed to solve the plane strain [36] and axisymmetric [37, 38] stability problems in soil mechanics. Extension of the method to the more general case of noncoaxiality has also been made [39]. Innovation of the extension of the method to the more general three-dimensional case has been

presented here, in this paper. The capability of the method in assessing the three-dimensional stability of slopes that are curved in plan has also been demonstrated.

2. THEORY

a) Basic assumptions

Consider an element of soil between two neighboring intermediate principal stress planes in a three-dimensional problem (Fig. 1). The local coordinate system (x, z) is assumed so that the z-axis is located where these two close σ_2-planes intersect. It is obvious that at the failure state, the flow of soil occurs in σ_2-plane since it is the largest Mohr circle with diameter $\sigma_1 - \sigma_3$ that touches the Mohr-Coulomb failure envelope at such a state. With the analysis of boundary value problems of soil stability type in these planes, as it is usual in the methods of stress characteristics or zero extension lines, the stress and velocity fields for the three dimensional problem can be simply obtained. All we have to do is to find the orientation of these planes for the three-dimensional problem at hand. For numerous three-dimensional problems in homogeneous isotropic soils, these planes can be assumed to be straight, so that once their orientation is obtained along a closed curve, their orientation would be known everywhere in the three-dimensional space. In two-dimensional problems like plane strain or axial symmetry, the orientation of σ_2-planes is normal to the boundary of the loaded area as the perimeter of a footing. This raises the notion of keeping the same condition for three-dimensional problems; i.e. for the vertically loaded area, σ_2-planes are normal to the boundary curve of the loaded area. The orientation of σ_2-planes for the general case of an inclined load over the area is considered in the next section.

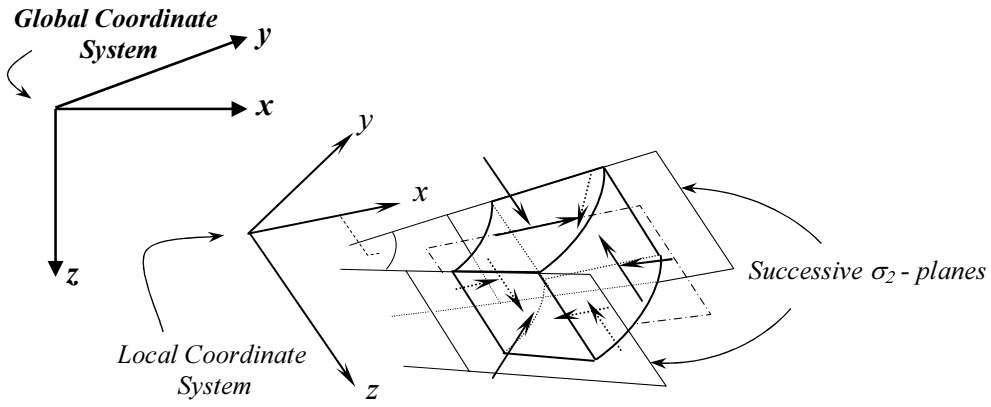

Fig. 1. Stress components acting on an element of soil between successive σ_2-planes

b) Orientation of σ_2-planes for the case of inclined load

Similar to the two-dimensional problems, we would have singularities at the edge of the loaded area. These are the points at which abrupt changes in the direction of ε_1, and hence in the magnitude of stress, take place. It is assumed that a rigid wedge is produced under the loaded area by the action of applied load, and is trapped between the adjacent plastic zones in the soil. The surface of such a wedge is generated by the velocity characteristics (zero extension lines) which are assumed to be straight. These lines cross the direction of ε_1 at an angle of $\xi = 45 - \nu/2$. The direction of ε_1, considered to be unique for the trapped wedge, can simply be obtained from the orientation and inclination of the applied load. Consider the total applied load Q, inclined at an angle δ with respect to normal to the loaded surface. This can be considered as the resultant of a uniformly distributed average traction q, applied to the surface of the loaded area at the same angle δ. Fig. 2 shows the Mohr circle for an element of soil in the wedge at a σ_2-

plane parallel to the applied force and right adjacent to the edge (point of singularity). It is clear that the direction of ε_1 makes an angle $\kappa/2$ with the normal to the surface of the loaded area.

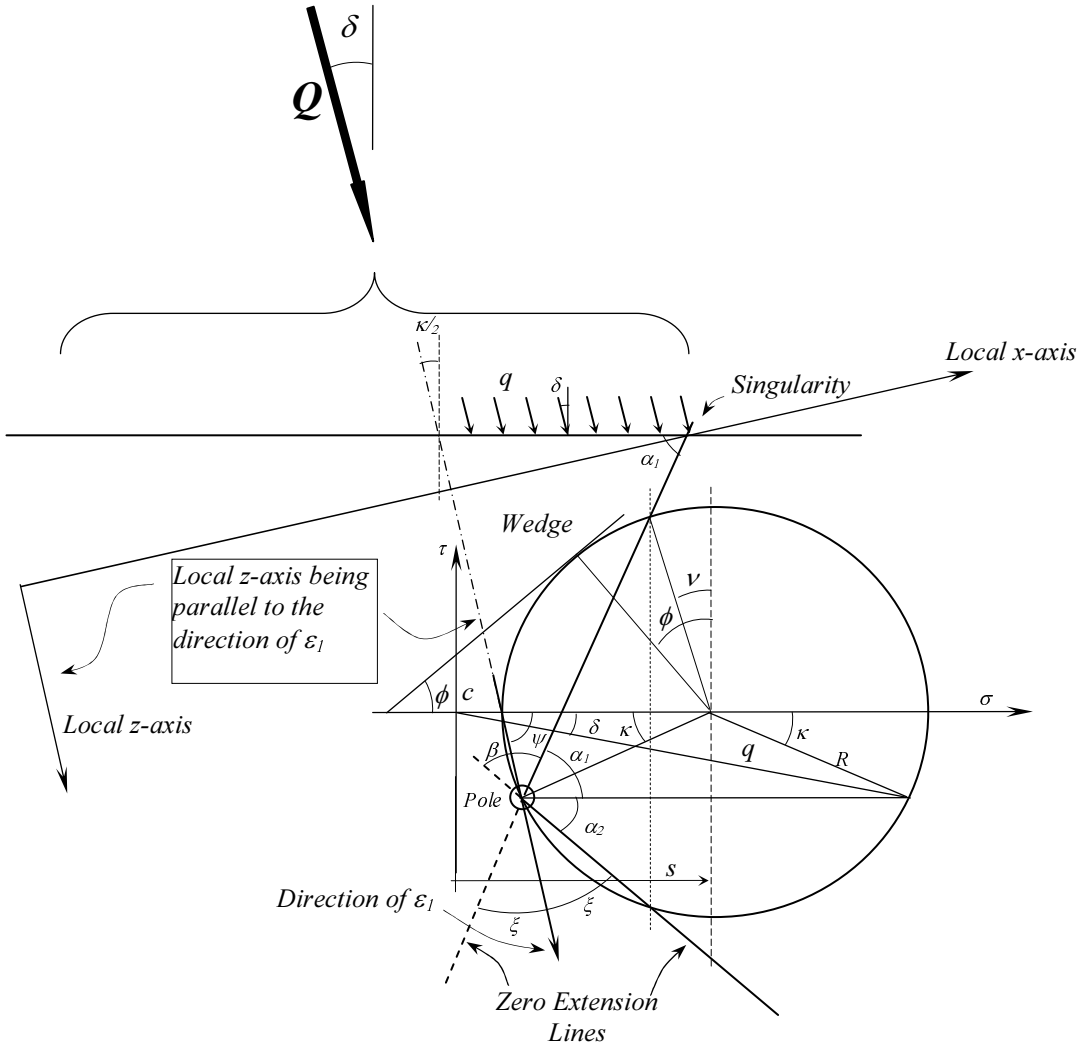

Fig. 2. Mohr circle for an element of soil in the wedge adjacent to the point of singularity

Considering the geometry of the Mohr circle shown in Fig. 2, the angle κ can be expressed in terms of δ as:

$$\kappa = \sin^{-1}\left(\frac{s}{s\sin\phi + c\cos\phi}\sin\delta\right) + \delta \tag{1}$$

Figure 2 also shows that the minimum and maximum values for κ are 2δ and $\sin^{-1}\left(\frac{\sin\delta}{\sin\phi}\right)+\delta$, respectively. Eq. (1) indicates that except in the extreme cases just mentioned, the method of finding κ from δ in a more general case where the soil has cohesion requires an iterative procedure. This is because the value of κ depends on the average stress s, which in turn depends on κ. In each step a new value of κ is the calculated and used for the calculation of s which itself is used in Eq. (1) for calculation of κ in the next step. The iteration proceeds until convergence in the value of κ is obtained.

The geometry of the trapped wedge under the loaded area is such that the local z-axes in the σ_2-planes make the same angle $\kappa/2$ with the normal to the surface of the loaded area. The local x-axis in each σ_2-

plane is perpendicular to the local z-axis, and passes through the point at which the edge of the loaded area crosses the σ_2-plane. This has been typically shown in Fig. 2.

c) Methodology of finding the σ_2-plane at the points on the perimeter of the loaded area

The unique value of angle $\kappa/2$ which depends on δ and the stress state can now be used for construction of the trapped wedge under the loaded area. Fig. 3 shows the perimeter of the loaded area when rotated by the angle $\kappa/2$ so that the direction of ε_1 is vertically downward. The perimeter of the loaded area in such a diagram would be, in general, a space curve. Consider A as a typical point on the perimeter curve. We want to find the σ_2-plane passing through this point and the local z- and x-axes together with the zero extension line in that plane. An inverted right circular cone at A with an apex angle of $\beta=90-\nu$ would be the locus of straight lines that pass through A and make $\xi=45-\nu/2$ with the direction of ε_1. These straight lines are the generators of the cone and the zero extension line that we want is one of them. This cone, together with its axis, can be considered as a conical plumb bob attached to its string (cone axis), held vertically at the edge of the slot made by the perimeter curve (Position *C-1* in Fig. 3). If it is let to penetrate inside the slot in a way that it always has contact at A (*C-2* in Fig. 3), the trace of its vertical axis defines the σ_2-plane passing through point A. In this way the cone slips down along one of its generators which is the zero extension line that we want. This line has been shown by the dashed line in Fig. 3. The extent of this slip is up to the state where the cone gets in touch with the other side of the slot at some point like B. The local x-axis would be drawn perpendicular to the axis of the cone in that σ_2-plane, in a way that it passes through A as well. The local z-axis would be the axis of the cone at a state it has slipped down to the extent that its curvature at the point of contact A is the same as the curvature of the perimeter curve (*C-3* in Fig. 3). In fact, the wedge is formed by the movement of such a vertical cone in the slot in a way that it always has at least two points of contact with the perimeter curve.

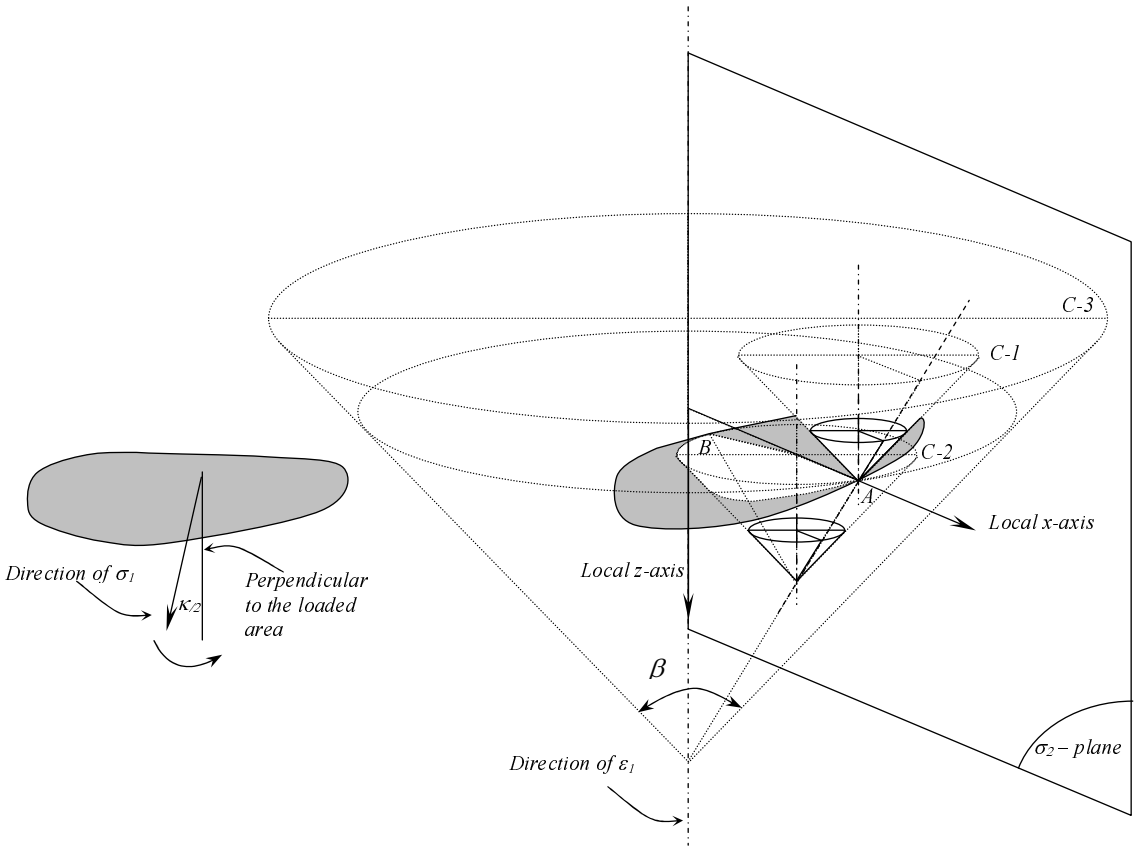

Fig. 3. Geometric considerations of the trapped wedge under the loaded area

The geometric considerations for finding the σ_2-planes, local coordinate axes, and zero extension line mentioned here, have been incorporated into computer-code numerical routines to give the geometric properties of the wedge under the loaded area bounded by a definite perimeter curve [40].

d) Equilibrium-yield equations in a typical σ_2-plane

Once the location of the local *z*- and *x*-axes in all σ_2-planes passing through different points of the perimeter curve is found, the limiting equilibrium state of the problem can be investigated. The soil media between two successive σ_2-planes is treated as a rough retaining wall problem at the state of axial symmetry. The side of the wedge plays the role of the wall. This is typically shown in Fig. 4. The solution of such a problem, which has been well investigated in [37], is used here as a fundamental tool for obtaining the stress field in the failure zone in each σ_2-plane. The local *z*-axis in each of these planes plays the role of local axis of symmetry for this so called *locally axi-symmetric problem*. The equilibrium-yield equations along the velocity characteristics would be in the following form [37]:

Along the (-) ZEL:

$$ds + \frac{\partial T}{\partial \varepsilon^+} d\varepsilon^- - \frac{2T}{\cos\nu}\left(d\psi - \sin\nu \frac{\partial \psi}{\partial \varepsilon^+} d\varepsilon^- \right) = \left[f_x \cos(\psi - \xi) + f_z \sin(\psi - \xi) \right] d\varepsilon^-$$

Along the (+) ZEL:

$$ds + \frac{\partial T}{\partial \varepsilon^-} d\varepsilon^+ + \frac{2T}{\cos\nu}\left(d\psi - \sin\nu \frac{\partial \psi}{\partial \varepsilon^-} d\varepsilon^+ \right) = \left[f_x \cos(\psi + \zeta) + f_z \sin(\psi + \zeta) \right] d\varepsilon^+ \tag{2}$$

In the above equations, T is the measure of the radius of Mohr circle at failure which is equal to $s\sin\phi + c\cos\phi$. ψ is the angle between the positive direction of *x*-axis and ε_1, measured clockwise. The zero extension lines make the angle $\xi = 45 - \nu/2$ with the direction of ε_1. It has to be mentioned that the above equations are written in local coordinate system and f_x and f_z are defined by the following equations:

$$f_x = X - \frac{T}{x}(1 + \cos 2\psi)$$

$$f_z = Z - \frac{T}{x}\sin 2\psi \tag{3}$$

X and *Z* in Eqs. 3 include body, seepage, and inertial forces in *x* and *z* directions respectively. Details of such derivations are provided in [37, 39].

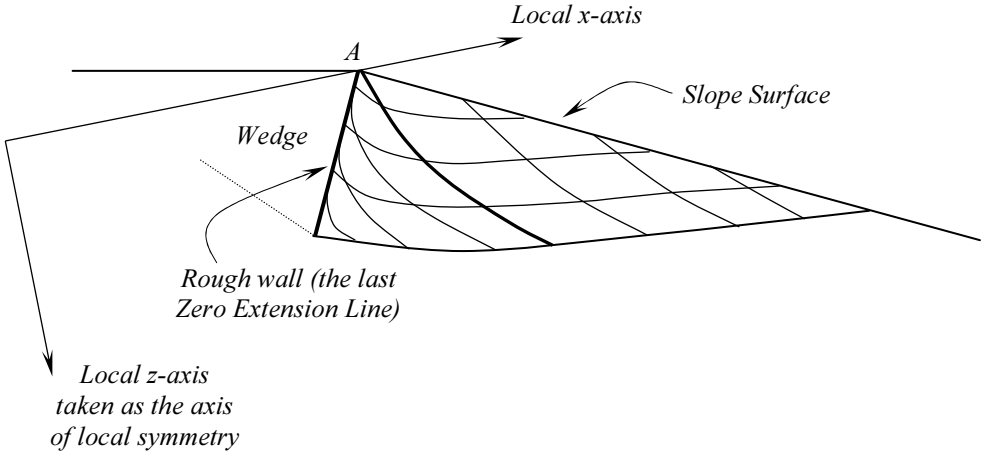

Fig. 4. Typical plastic zone and velocity characteristics near the wedge in a σ_2-plane

Integration of these equations along the zero extension lines results in determination of the stress field within the failure zone in each of the σ_2-planes. In this way, the stress field in the plastic zone around the wedge is determined. This information allows calculation of traction forces that act on the surface of the wedge. Under the action of these forces together with the body, inertial and seepage forces, the equilibrium of the wedge is assessed and the amount of load that can be applied to the load area at the state of limiting equilibrium is calculated. Such procedure has been implemented into a computer program, *Slope3D8*, the flowchart of which is shown in Fig. 5. The program has been specially developed to assess the three-dimensional stability of slopes that are curved in the plan. The intention has also been to assess the aggravating effect of outward centrifugal force resulting from the movement of traffic in curved routes on the stability of the slope. Parameters of the model in a circular segment have been depicted in the three-dimensional diagram of Fig. 6. The problem is assumed to be symmetric with respect to the global ***x-z*** plane in which the load Q lies. Strength of soil is also mobilized on the other side of the wedge away from the slope. Therefore, a strength mobilization factor, m, is considered to account for the amount of soil strength that is mobilized on that side. The value of m is obtained via an iterative procedure in the code to have the ultimate load, Q, inclined at the known angle, δ, with the normal to the surface (Fig. 6).

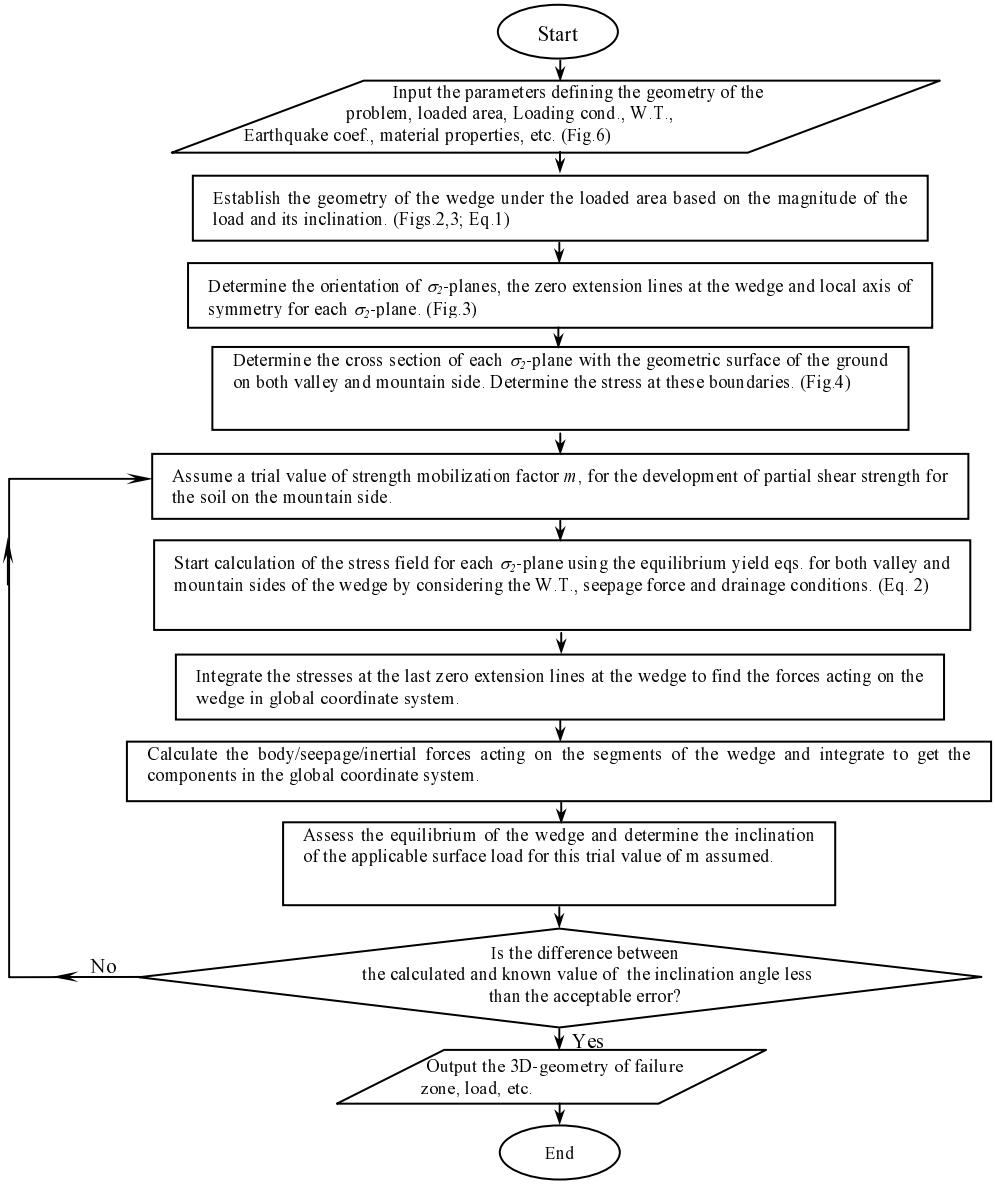

Fig. 5. Flow chart of the program

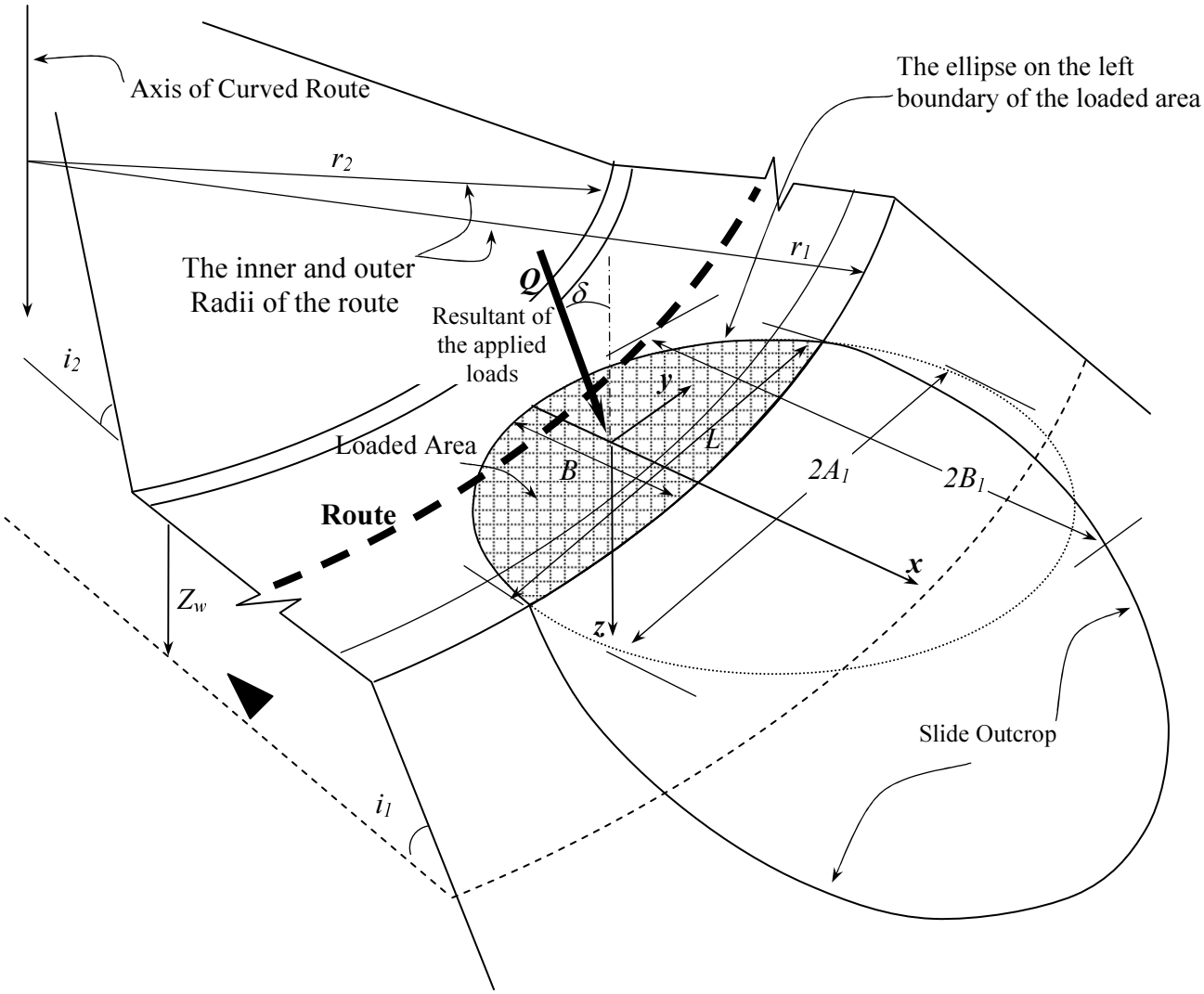

Fig. 6. Geometric parameters of the problem introduced to the computer code

Drained conditions are analyzed by the seepage force method which is simpler for incorporation into the equilibrium-yield equations. The seepage forces which are used as the body forces in the equations are obtained by multiplying the hydraulic gradient at each point by the unit weight of water. They are used together with the buoyant unit weight in the equations. It is worthy to note that in contrast to limit equilibrium or limit analysis methods, the algorithm for the solution of the problem by the presented method does not involve any search procedure for finding the geometry of a critical slip surface giving a minimum or assumed factor of safety. Here, like the method of stress characteristics the geometry of the failing zone and the bottom slip line are part of the solution obtained during the solution of the governing equations.

3. EXAMPLES OF APPLICATION

The following examples are provided here, to show the features and capabilities of the model.

3.1 Example 1. In this example a three-dimensional mechanism is analyzed in a slope of cohesive soil which is straight in plan. The shear strength of clay is 60 kPa and the unit weight is 17kNt/m^3. The boundary of the loaded area at the left is circular with a radius of 30 m. The width of the loaded area at the middle section is 20 m. The lateral and vertical coefficients of earthquake are 0.1 and 0.05 (vertically

upward), respectively. The inclination of the load with respect to the vertical in this case would be δ=6°. Fig. 7 shows the three dimensional schematic diagram of failure mechanism when the slope angle is 30°. Safety factor is applied to the shear strength of the soil and the ultimate load is calculated for different slope angles. The calculated applicable load for different safety factors has been drawn vs. the slope angle in Fig. 8. As shown, the applicable load decreases with increase in slope angle or factor of safety.

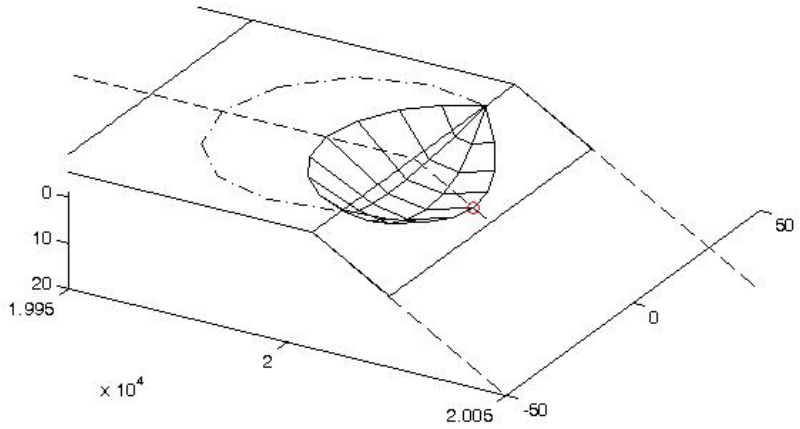

Fig. 7. Schematic diagram of failure mechanism for Example 1

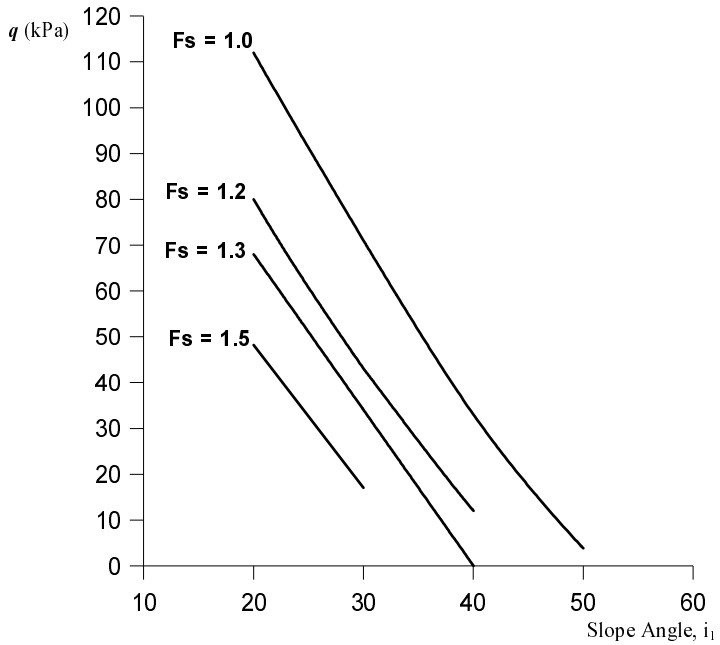

Fig. 8. The applicable crest load as a function of 3D-safety factor and slope angle for Example 1

3.2 Example 2. A slope of relatively cohesionless soil in drained condition has been analyzed in this example. The slope is 35° with respect to horizon and is curved in plan. It supports a curved route of 15m width with an outer radius of 60m. The hill on the left side of the route has also been assumed to have the same slope. The width of the loaded area at the middle is 10m. Its left side boundary is an ellipse with B1=30m and A1=75m (Fig. 6). The soil has been assumed to behave associatively with ϕ=30° and c=20kPa in drained condition. The depth of the water table is 1.0m below the route. The dry and saturated unit weights of soil are 17 and 20 kNt/m^3 respectively. The moving traffic on the curved route has been

assumed to produce a centrifugal force that causes the resultant Q to make an angle of 12^o with the normal to the loaded area, i.e., $\delta = 12^o$. The flow net for this drained condition has been assumed to be uniform with parallel flow lines making the angle i_3 with the horizon. A range of $i_3=0$ (horizontal flow) to $i_3= i_1 =35^o$ (parallel to slope-flow) has been investigated to see the effect of flow direction on the stability. Fig. 9 shows the failure zone for this example. The outcrop of the zone influenced by the failure has also been shown on the other side of the loaded area in this figure. Fig. 10 shows the variation of ultimate load with the direction of flow in the slope. As shown, the horizontal flow affects the instability of the slope more than the parallel flow.

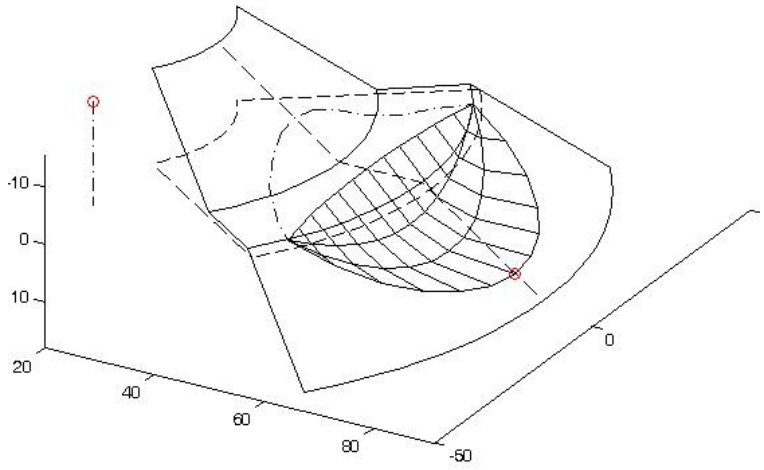

Fig. 9. Schematic diagram of failure mechanism for Example 2

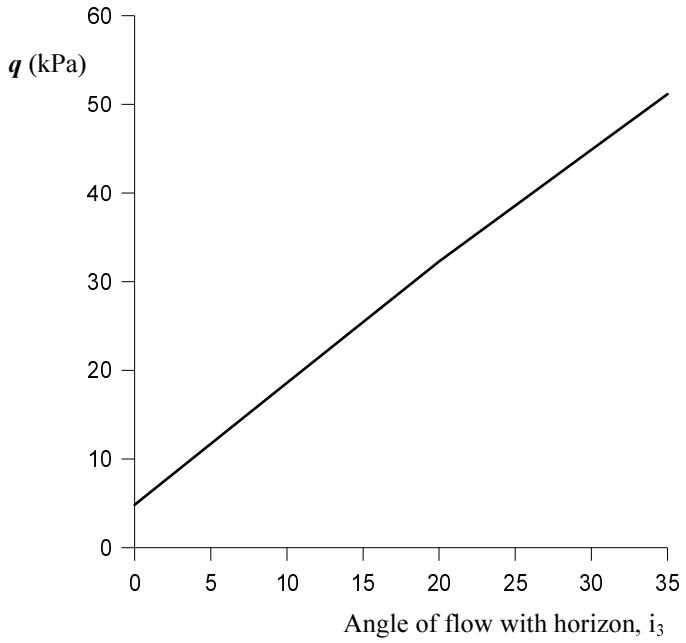

Fig. 10. The applicable crest load as a function of the angle of water-flow for Example 2

3.3 Example 3. A concave slope of relatively cohesionless soil in drained condition has been analyzed in this example. The slope angles for the valley side and mountain side are assumed to be the same and equal to 30^o. It supports a curved route of 10m width with outer and inner radii of 60 and 50 meters,

respectively. The width of the loaded area at the middle is 7m and its length is 40m. Its left side boundary is assumed to be elliptic. The ratio of its diagonals has been assumed 0.56 (Fig. 6). The soil has been assumed to behave associatively with ϕ=35^{o} and c=6.66kPa in drained condition. The depth of the water table has been varied in this example to see its influence on the stability of the slope. The dry and saturated unit weights of soil are 16 and 21 kNt/m^3 respectively. The flow net for this drained condition has been assumed to be parallel to the slope surface. Fig. 11 shows the failure zone for this example when the water level is at mid-height of the slope. The ultimate loads for different levels of water table in the slope have been shown in Fig. 12. As shown, the load-bearing capacity of the slope decreases to one third by rise of water to the level of crest.

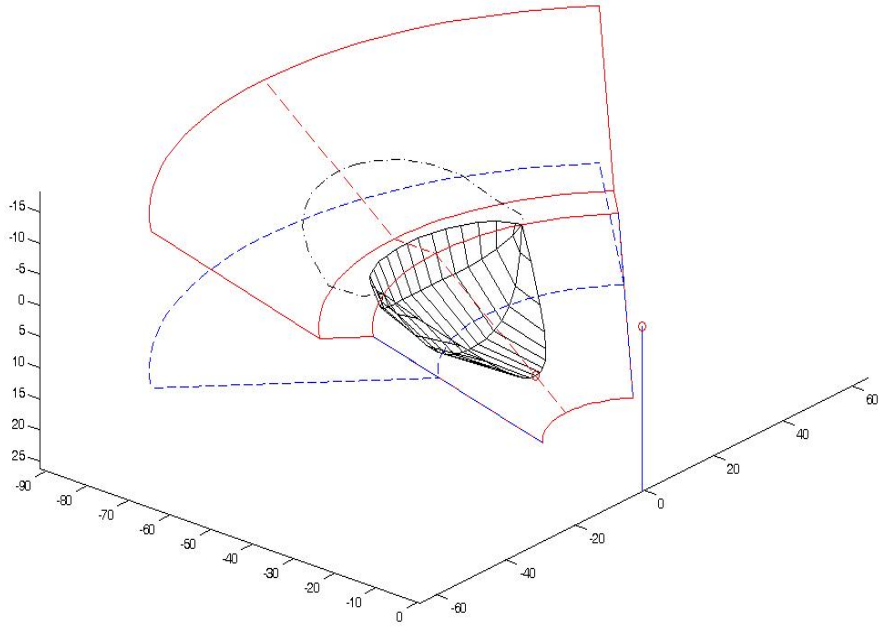

Fig. 11. Schematic diagram of failure mechanism for Example 3

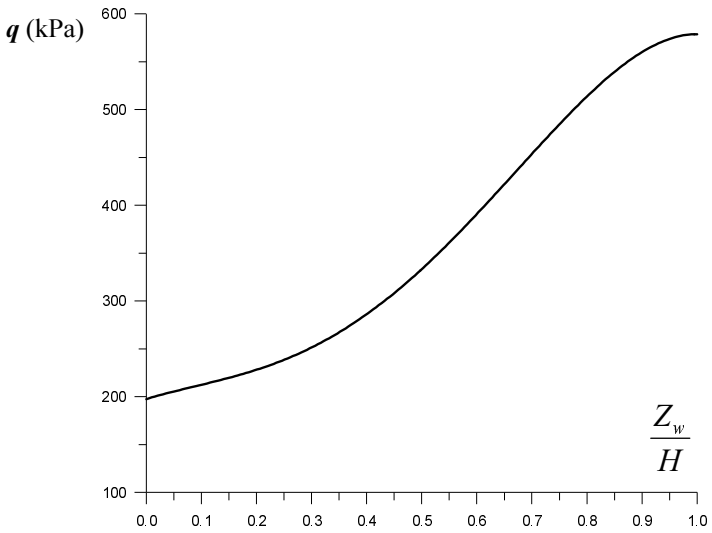

Fig. 12. The applicable crest load as a function of water-level in slope of Example 3

4. COMPARISON WITH PREVIOUS WORKS

The simple three-dimensional zero extension method (3D-ZELM) presented here is limited to homogeneous soils. It is not as versatile as the limit equilibrium method (LEM) or limit analysis method (LAM) to consider nonhomogeneous slopes. Some points should be mentioned before we enter the discussions about comparing the results of this model with those of the others: First of all, this method investigates the 3D-instability caused by the application of load to a limited area of the crest. As mentioned before, there are other sources for 3D-instability. Case histories recorded in the literature are limited to those in which a natural or man-made 3D weak surface or material non-homogeneity is present, or the slides in narrow valleys. Works done by other methods on the instability under the crest load are rare and are limited to those by the upper bound method of limit analysis (LAM). This method tries to provide the least upper bound to the true collapse load by examining different collapse mechanisms and using an optimization procedure. The results obtained by this method have been selected for comparison with the ZELM. It should be mentioned that the 3D-ZELM satisfies the equilibrium condition at a limiting state and we expect it to give lower values for the ultimate load compared to LAM which gives the upper bound to the true collapse load. Moreover, the governing equations in the ZELM form a closed set so that no optimization is involved in the solution of the problem. Secondly; it should be mentioned that the geometries of the loaded areas at the crest for three dimensional LAM and ZELM are not exactly the same. Attempts have been made to resemble the rectangle of load area in LAM by semi-ellipse of the same area and length. This may be the source of some of the differences between the compared results of these methods. Thirdly; we should note that the 3D-ZELM developed here does consider the effect of soil conditions on the counter side of the slope in the analysis, but the other 3D models do not. Mobilization of some strength in the soil on the counter side of the slope contributes to the instability of the slope side. This effect has only been observed in the two dimensional LAM work of Saran et. al. [41] to which we have compared our 2D results.

Although the model has the advantage of considering a slope on the counter side (as a hill or mountain), this option has been put aside in the comparisons to make the conditions the same as other approaches. Therefore, the values of r_2 and i_2 have been set equal to zero to resemble a flat crest for the slope (Fig. 6). The value of r_1 is taken very large to resemble a slope that is straight in plan. When two dimensional results are required, the length of the loaded area, L, is also taken very large in order to suppress the effect of ends as much as possible (see Fig. 6).

The results of the program have been confirmed by comparison with the rigorous results for the case of no slope. For the case of a purely cohesive soil of cohesion c, a value of 5.14 is obtained for the ratio q/c which is identical with the theoretical value of $N_c=\pi+2$ at $\phi=0$. The same result is obtained when the soil density is also taken into account. As we know, the value of N_γ is zero for $\phi=0$. In the case of slope, the ratio q/c for purely cohesive soils depends on the slope angle. It also depends on the dimensionless ratio $\gamma B/c$, as well. Saran et. al. have provided the result of LAM for the case of $\gamma B/c=0$ in which the effect of counter side has also been considered [41]. Comparison of their results with those of ZELM, as shown in Fig. 13, indicates that LAM gives higher values for the load as expected. Results of analysis by the ZELM indicate that q/c decreases almost linearly with increase in slope angle i_1 (Fig. 13). The rate of this decrease is higher for higher values of $\gamma B/c$. The theoretical value of $q/c=5.14$ obtained for all values of $\gamma B/c$ at $i_1=0$ has also been shown in the figure. The solution for the case of slope with no-crest load is obtained by the limiting states where q/c approaches zero for every value of $\gamma B/c$. These results have been shown in the form of $\gamma H/c$ vs. slope angle in Fig. 14. Comparison with the result of the slip circle method of Taylor [42] indicates lower values for the ZELM.

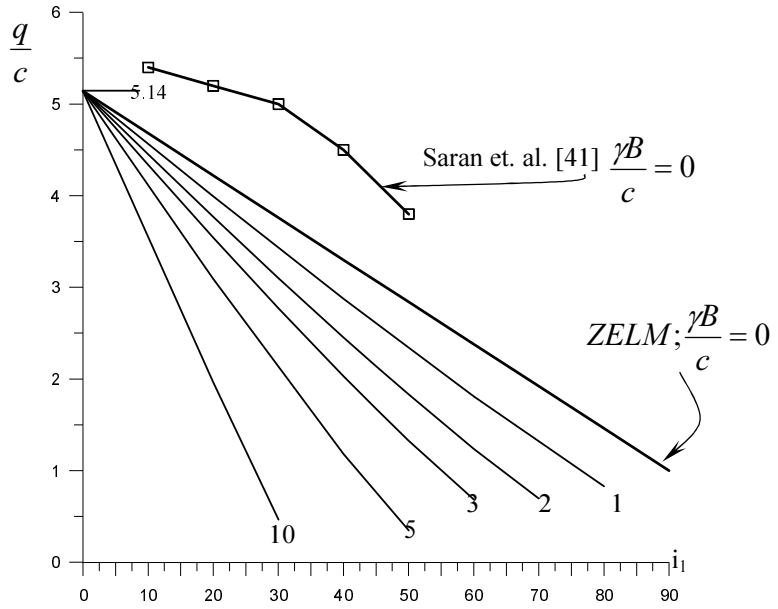

Fig. 13. Comparison of 2D results of the ZELM and LAM of Saran, et. al. for cohesive soils

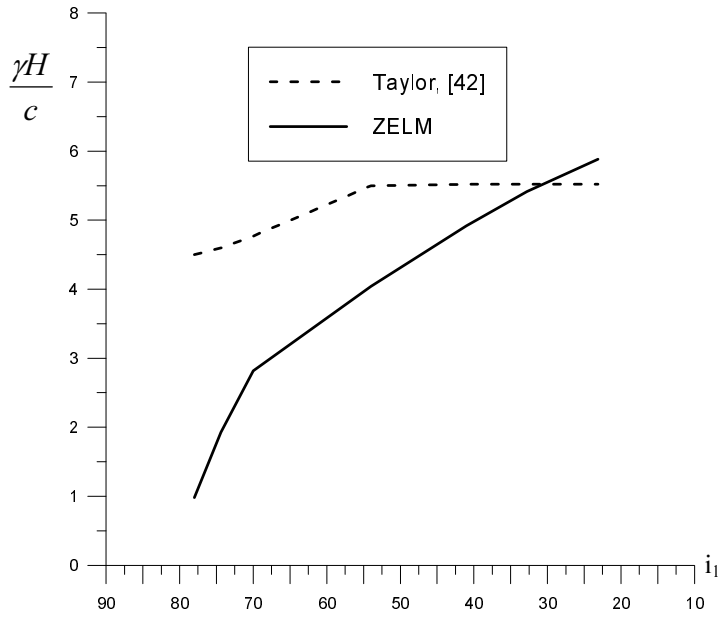

Fig. 14. Comparison of 2D results of the ZELM and Taylor's slip-circle method for cohesive soils

For the case of purely frictional soils, the value of q is divided by $0.5\gamma B$ to make it dimensionless. When the slope angle is zero, the value of $q/0.5\gamma B$ is nothing but N_γ, which is only a function of soil friction angle. Table 1 compares the results with those of LAM of Saran et al. [41] and SCM of Bolton and Lau [43]. The data of Hansen and Vesic for N_γ is also included. The comparison indicates that the ZELM results are close to the SCM of Bolton and Lau. The upper bound values of Saran et al. [41] are higher than the others. Fig. 15 shows the variation of the dimensionless ratio $q/0.5\gamma B$, vs. slope angle for soils of different friction angle. The results of Saran et. al. have also been shown in the figure. As expected, their results are higher than those obtained by the ZELM.

Michalowski [19] has investigated the 3D stability of locally loaded slopes by the upper bound-LAM. The case of purely frictional soils with 30^o friction angle is shown in Fig. 16. The loaded area considered is a rectangle adjacent to the slope with a length to width ratio of 2. Askari [20], and Farzaneh and Askari, [21] have used the same method but have considered a more complicated collapse mechanism and

obtained a lower upper bound value (by 10%). Results obtained by the 3D-ZELM have also been shown in the same figure. These results have been produced using a semi-elliptic shape loaded area that is equal to their rectangle in area and length. The results indicate higher values by the 3D-LAM in comparison to 3D-ZELM as is expected. Some of the differences between these results may be attributed to the effect of soil on the slope-counter side. As mentioned before, this effect, which is more pronounced for lower slope angles, has not been considered in 3D limit analyses.

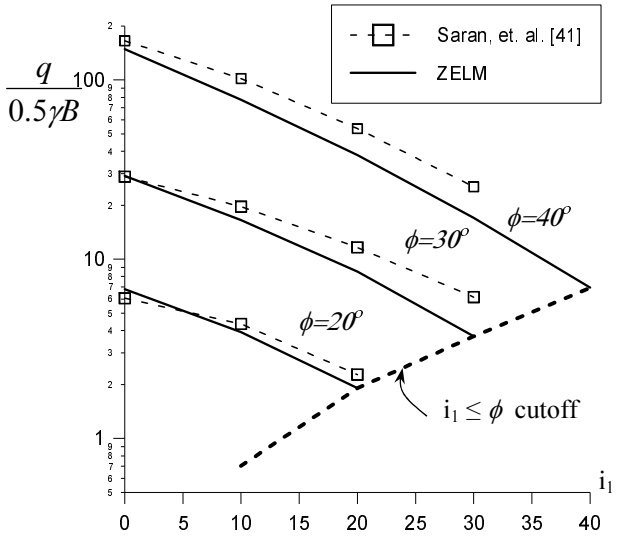

Fig. 15. Comparison of 2D-results of the ZELM and LAM of Saran, et. al. for frictional soils

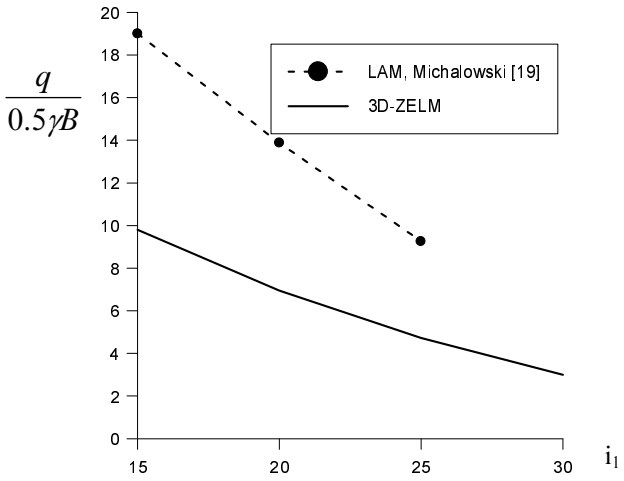

Fig. 16. Comparison of 3D-results of the ZELM and LAM of Michalowski for frictional soil with ϕ=30

Figure 17 compares the results of 3D-ZELM with those of 3D-LAM in the case of c-ϕ-soils. Comparison is made in cases where the dimensionless ratio, $\gamma B/c$, is equal to 0.25 and 1.25 considered by Michalowski [19]. The figure also includes the case of ϕ=0, which represents a purely cohesive soil. The length to width ratio of the rectangle of the loaded area is again 2.0. As shown, the dimensionless load ratio q/c decreases with increase in slope angle and the results by 3D-ZELM are generally lower that those obtained by 3D-LAM.

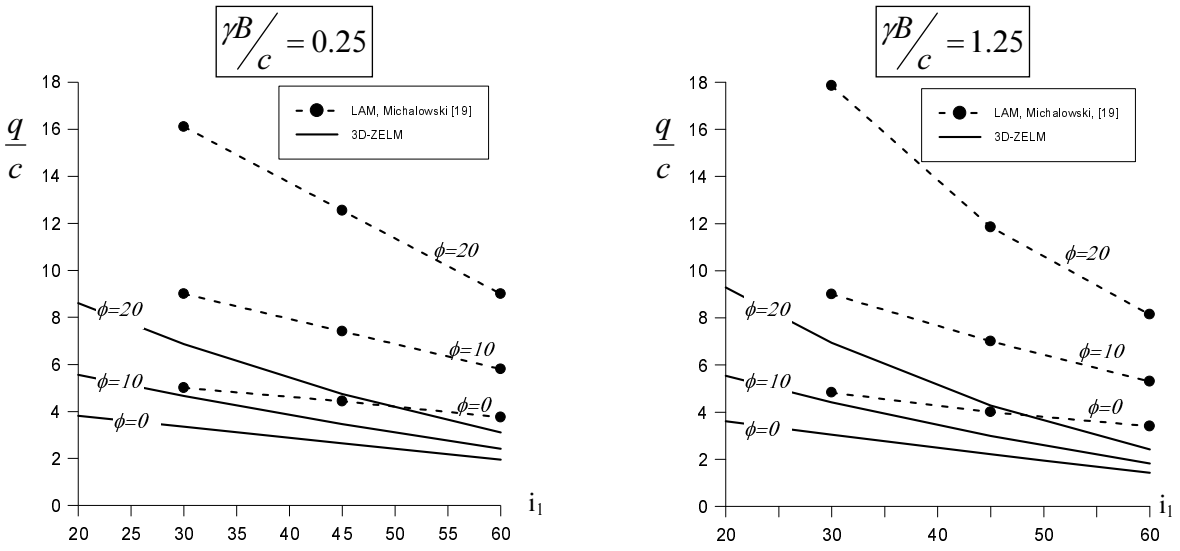

Fig. 17. Comparison of 3D-results of the ZELM and LAM of Michalowski for c-ϕ-soils

Table 1. Comparison of N_γ values as suggested by different researchers or methods

ϕ	$N_\gamma = q/0.5\gamma B$				
	Hansen	Vesic	Bolton and Lau (1993), [43]	ZELM	Saran et. al. (1989), [41]
5	0.1	0.4	0.62	1.27	
10	0.4	1.2	1.71	2.11	1.14
15	1.2	2.6	3.17	3.67	2.74
20	2.9	5.4	5.97	6.69	6.05
25	6.8	10.9	11.6	12.83	13.12
30	15.1	22.4	23.6	26.15	28.89
35	33.9	48.03	51.0	57.52	66.59
40	79.4	109.3	121	139.8	165.39
50	567.4	761.3	1052	1285	

5. SUMMARY AND CONCLUSION

The simple three-dimensional model presented here, which was based on the zero extension line method, can be used for stability analysis in soil engineering. This model is relevant to conditions where the local loading is the main cause of the three-dimensional failure. A rigid wedge is assumed to form under the loaded area and the characteristic planes in which the flow of soil takes place are obtained by geometric considerations of the problem. The equilibrium-yield equations are integrated along the velocity characteristics (zero extension lines) in these planes and the failure zone is obtained. Examples presented indicate that the model also considers the effect of the soil on the counter side of the slope on the stability. The capabilities of the model in analyzing stability of straight and curved slopes in the plan have also been shown. Lateral forces due to earthquake or moving traffic in curved routes can also be modeled by the method. The aggravating effect of seepage force due to flow of water in the slope under drained conditions can also be investigated. Comparison of the results with those of LAM indicates that the predicted ultimate loads of the ZELM are generally lower than those of upper-bound-LAM. The greater difference between the results of these two models in the 3D-problem is because in the presented 3D-LA approaches, the aggravating effect of soil at the counter side of the slope on its stability has not been considered in

modeling. It is concluded that the simple 3D zero extension line model presented here provides a useful tool for the 3D-analysis of stability problems in soil engineering.

Acknowledgement- This paper is part of a research project supported by research departments of Shiraz University and the Ministry of Road and Transportation. The authors wish to thank the officials of these organizations for their support in completing the research work. Assistance of Messrs Arvin and Nikooee in providing some of the literature of the subject is also acknowledged.

REFERENCES

1. Sherard, J. L., Woodward, R. J., Gizienski, S. F. & Clevenger, W. A. (1963). *Earth and earth-rock dams*. John Wiley & Sons, Inc., NY, 725 pp.
2. Lambe, T. W. & Whitman, R. V. (1969). *Soil mechanics*. John Wiley & Sons, NY, 553 pp.
3. Anagnosti, P. (1969). Three-dimensional stability of fill dams. *Proceedings, of the 7th International Conference on Soil Mechanics and Foundation Engineering*, Mexico, Vol. 2, pp. 275–280.
4. Azzouz, A. S. & Baligh, M. M. (1978). Three-dimensional stability of slopes. Research Report R78-8, Order No. 595, Dept. of Civil Eng., Massachusetts Institute of Technology, Cambridge, Mass., 349 pp.
5. Azzouz, A. S. & Baligh, M. M. (1983). Loaded areas on cohesive slopes. *J. Geotech. Eng. Div., ASCE*, Vol. 109, No. 5, pp. 726-729.
6. Gens, A., Hutchinson, J. N. & Cavounidis, S. (1988). Three dimensional analysis of slides in cohesive soils. *Geotechnique*. Vol. 38, No. 1, pp. 1-23.
7. Hovland, H. J. (1977). Three dimensional slope stability analysis method. *J. Geotechnical Eng. Div., ASCE*, Vol. 103, No. 9, pp. 971-986.
8. Chen, R. H. & Chameau, J. L. (1982). Three dimensional limit equilibrium analysis of slopes. *Geotechnique*, Vol. 32, No. 1, pp. 31-40.
9. Chen, Z., Mi, H., Zhang, F. & Wang, X. (2003). A simplified method for 3D slope stability analysis. *Can. Geotech. J.*, Vol. 40, pp. 675-683.
10. Jiang, J. C. & Yamagami, T. (2004). Three-Dimensional slope stability analysis using an extended Spencer method. *Soils and Foundations*, Vol. 44, No. 4, pp. 127-135.
11. Leshchinsky, D. & Baker, R. (1986). Three dimensional analysis of slope stability. *Soils and Foundations*, Vol. 26, No. 4, pp. 98-110.
12. Leshchinsky, D. & Huang, C. C. (1992). Generalized slope stability analysis: interpolation, modification and comparison. *J. Geotechnical Eng. Div., ASCE*, Vol. 118, pp. 1748-1764.
13. Ugai, K. (1988). Three-dimensional slope stability analysis by slice methods. *Proc., 6th Int. Conf. on Numer. Methods in Geomech.*, A. A. Balkema, Rotterdam, Netherlands, pp. 1369-1374.
14. Byrne, R. J., Kendall, J. & Brown, S. (1992). Cause and mechanism of failure of Kettleman Hills Landfill B-19, Phase I-A. Instability and Performance of Slopes and Embankments– II, American Society of Civil Engineers, Geotechnical SpecialTechnical Publication No. 31, Edited by R.B. Seed and R.W. Boulanger. Vol. 2, pp. 1188–1215.
15. Hungr, O., Salgado, F. M. & Byrne, P. M. (1989). Evaluation of three dimensional method of slope stability analysis. *Can. Geotech. J.*, Vol. 26, No. 4, pp. 679-686.
16. Huang, C. C. & Tsai, C. C. (2000). New method for 3D and asymmetrical slope stability analysis. *J. Geotechnical Eng. Div., ASCE*, Vol. 126, No. 10, pp. 917-927.
17. Huang, C. C., Tsai, C. C. & Chen, Y. H. (2002). Generalized method for three dimensional slope stability analysis. *J. Geotechnical Eng. Div., ASCE*, Vol. 128, No 10, pp. 836-848.

18. Yu, H. S., Salgado, R., Sloan, S. W. & Kim, J. M. (1998). Limit analysis versus limit equilibrium for slope stability. *J. Geotech. and Geoenv. Eng. Div*., Vol. 124, No. 1, pp. 1-11.
19. Michalowski, R. L. (1989). Three dimensional analysis of locally loaded slopes. *Geotechnique*. Vol. 39, pp. 27-38.
20. Askari, F. (1999). A limit analysis method for three dimensional seismic stability of nonhomogeneous slopes. PhD thesis, Faculty of Eng., University of Tehran, Tehran, Iran.
21. Farzaneh, O. & Askari, F. (2003). Three dimensional analysis of nonhomogeneous slopes. *J. Geotech. Eng., ASCE*, Vol. 129, No. 2, pp. 137-145.
22. Donald, I. B. & Chen, Z. (1997). Slope stability analysis by the upper bound approach: Fundamentals and methods. *Can. Geotech. J*., Vol. 34, pp. 853-862.
23. Giger, M. W. & Krizek, R. J. (1975). Stability analysis of vertical cut with variable corner angle. *Solis and Found*., Vol. 15, No. 2, pp. 63-71.
24. Chen, Z., Wang, X., Haberfield, C., Yin, J. H. & Wang, Y. (2001). A three-dimensional slope stability analysis method using the upper bound theorem. Part I: Theory and methods. *Int. J. Rock Mech. and Mining Sciences*, Vol. 38, pp. 369-378.
25. Chen, Z., Wang, J., Wang, Y., Yin, J. H. & Haberfield, C. (2001). A three-dimensional slope stability analysis method using the upper bound theorem. Part I: Numerical approaches, applications and extensions. *Int. J. Rock Mech. and Mining Sciences*, Vol. 38, pp. 379-397.
26. Drescher, A. & Detournay, E. (1993). Limit load in translational failure mechanisms for associative and non-associative materials. *Geotechnique*, Vol. 43, No. 3, pp. 443-456.
27. Sokolovski, V.V. (1960). *Statics of soil media*. Butterworth Scientific Publications: London.
28. Atkinson, J. H. (1981). *Foundation and slopes*. McGraw-Hill Book Company, New York, 382 pp.
29. Enoki, M., Yagi, N., Yatabe, R. & Ichimoto, E. (1991). Generalized limit equilibrium method and it's relation to slip line method. *Soils and Foundations*, Vol. 32, No. 2, pp. 1-13.
30. Harr, M. E. (1966). *Foundations of theoretical soil mechanics*. McGraw-Hill Book Company., New York, 381 pp.
31. Jahanandish, M. & Keshavarz, A., (2004). Stability of axially symmetric slopes in soil engineering. *Proc. Int. Conf. on Geotechnical Engineering*, Beirut, Lebanon, pp. 97-104.
32. Habibagahi, K. & Ghahramani, A. (1979). Zero extension line theory of earth pressure. *J. Geotech. Engng. Div., ASCE* 105, No. 7, pp. 881-896.
33. Ghahramani, A. & Clemence, S. P. (1980). Zero extension theory of dynamic passive pressure. *J. Geotech. Engng. Div., ASCE* 106, No. 6, pp. 631-644.
34. Jahanandish, M. (1988). *Zero extension line net and its application in soil mechanics*. M.Sc. thesis, Shiraz University, Shiraz, Iran.
35. Jahanandish, M., Behpoor, L. & Ghahramani, A. (1989). Load-displacement characteristics of retaining walls. *Proc. 12th ICSMFE, Vol. 1, Rio de Janeiro, Brazil, pp. 243-246.*
36. Anvar, S. A. & Ghahramani, A. (1997). Equilibrium equations on zero extension lines and its application to soil engineering. *Iranian Journal of Science and Technology, Transaction B, Engineering*, Vol. 21, B1, pp. 11-34.
37. Jahanandish, M. (2003). Development of the zero extension line method for axially symmetric problems in soil mechanics. *Scientia Iranica*, Vol. 10, No. 2, pp. 1-8.
38. Arvin, M. R. (2006). *Application of zero extension line method in analysis of axially symmetric slopes*. M.Sc. thesis, Shiraz University, Shiraz, Iran, 111 pp.
39. Jahanandish, M. & Eslami Haghighat, A. (2004). Analysis of boundary value problems in soil plasticity assuming non-coaxiality. *Iranian Journal of Science and Technology, Transaction B, Engineering*, Vol. 28, No. B5, pp. 583-594.

40. Jahanandish, M. (2008). *Three-dimensional stability analysis of slopes in curved routes*. Research Report 83B1T5P23(GEO), Transportation Research Institute, Ministry of Road and Transportation, I. R. IRAN.
41. Saran S., Sud, V. K. & Handa, S. C. (1989). Bearing capacity of footings adjacent to slopes. *J. Geotechnical Eng*., *ASCE*, Vol. 115, No. 4, pp. 553-574.
42. Taylor, D. W. (1940). Stability of earth slopes, Contribution to Soil Mechanics 1925-1940. Boston Society of Civil Engineers, Boston.
43. Bolton, M. D. & Lau, C. K. (1993). Vertical bearing capacity factors for circular and strip footings on mohr-coulomb soil. *Canadian Geotechnical Journal*, Vol. 30, No. 6, pp. 1024-1033.